Electronic Supplementary material for

SYNTHESIS OF NEW ZINC AND COPPER COORDINATION POLYMERS DERIVED FROM bis (TRIAZOLE) LIGANDS

Maria Cristina Al-Matarneh[1*], Alina Nicolescu[2*], Ioan-Andrei Dascalu[1], Sergiu Shova[3], Cristian-Dragos Varganici[1], Adrian Fifere[1], Ramona Danac[4], Ioana-Cristina Marinas[5].

*almatarneh.cristina@icmpp.ro, alina@icmpp.ro

[1]*Center of Advanced Research in Bionanoconjugates and Biopolymers, "Petru Poni" Institute of Macromolecular Chemistry of Romanian Academy, 41A Grigore Ghica Voda Alley, Iasi 700487, Romania*

[2]*NMR Laboratory, "Petru Poni" Institute of Macromolecular Chemistry of Romanian Academy, 41A Grigore Ghica Voda Alley, Iasi 700487, Romania*

[3]*Department of Inorganic Polymers, "Petru Poni" Institute of Macromolecular Chemistry of Romanian Academy, 41A Grigore Ghica Voda Alley, Iasi 700487, Romania*

4 Faculty of Chemistry, Alexandru Ioan Cuza University of Iasi, , 11 Carol I Bvd., Iasi 700506, Romania

[5]*Research and Development Department , SC Sanimed International Impex SRL, 6 Bucharest-Giurgiu street, 087040, Giurgiu, Romania;*

Table of contents	
1. FT-IR spectra of ligand L^1 and complexes $[CuL^1(NO_3)_2]_n$ and $[ZnL^1(NO_3)_2]_n$	**Figure S1**
2. FT-IR spectra of ligand L^2 and complex $[CuL^2NO_3]_n$.	**Figure S2**
3. ^{1}H-NMR spectrum corresponding to compound L^1, recorded in $CDCl_3$, at 600.1 MHz. Signals assignments are annotated on the figure.	**Figure S3**
4. ^{13}C-NMR spectrum corresponding to compound L^1, recorded in $CDCl_3$, at 150.9 MHz. Signals assignments are annotated on the figure.	**Figure S4**
5. H,H-NOESY spectrum recorded for compound L^1, with the insert showing the NOE correlation signals between 1,2,3-triazole proton and methoxy and butyl protons.	**Figure S5**
6. Detailed spectral region of ^{1}H,^{15}N-HMBC spectrum corresponding to compound L^1, showing the proton-nitrogen two and three bonds couplings used to determine the chemical shifts values for nitrogen atoms.	**Figure S6**
7. ^{1}H-NMR spectrum corresponding to compound L^2, recorded in $CDCl_3$, at 600.1 MHz. Signals assignments are annotated on the figure.	**Figure S7**
8. ^{13}C-NMR spectrum corresponding to compound L^2, recorded in $CDCl_3$, at 100.6 MHz.	**Figure S8**
9. Detailed spectral region of ^{1}H,^{15}N-HMBC spectrum corresponding to compound L^2, showing the proton-nitrogen two and three bounds couplings used to determine the chemical shifts values for nitrogen atoms.	**Figure S9**
10. ^{1}H-NMR spectrum corresponding to bisazide 2, recorded in $CDCl_3$, at 600.1 MHz. Signals assignments are annotated on the figure.	**Figure S10**
11. ^{13}C-NMR spectrum corresponding to bisazide 2, recorded in $CDCl_3$, at 100.6 MHz.	**Figure S11**
12. Overlapped ^{1}H-NMR spectra recorded at 400.1 MHz, in DMSO-d_6, for free L^1 (a), $[ZnL^1(NO_3)_2]_n$ complex (b) and $[CuL^1(NO_3)_2]_n$ complex (c). For cupper complex, significant line broadening causing the modification of splitting patterns is observed for all the signals.	**Figure S12**
13. Overlapped ^{13}C-NMR spectra recorded at 100.6 MHz, in DMSO-d_6, for free L^1 (a), $[ZnL^1(NO_3)_2]_n$ complex (b) and	**Figure S13**

$[CuL^1(NO_3)_2]_n$ complex (c). For cupper complex, significant line broadening is observed for 1,2,3-triazole cycle carbons.	
14. Overlapped ^{1}H-NMR spectra recorded at 400.1 MHz, in DMSO-d_6, for free L^2 (a) and $[CuL^2NO_3]_n$ complex (b). For cupper complex, significant line broadening causing the modification of splitting patterns is observed for two signals.	**Figure S14**
15. Bond distances (Å) and angles (°) for $[CuL^2NO_3]_n$ complex, $[ZnL^1(NO_3)_2]_n$ complex, L^1 ligand, $[CuL^1(NO_3)_2]_n$ complex, L^2 ligand.	**Table S1**
16. Powder XRD for $[CuL^1(NO_3)_2]_n$ complex.	**Figure S15**
17. TG-DTG curves of bisazide 2.	**Figure S16**
18. TG-DTG curves of ligand L^1	**Figure S17**
19. TG-DTG curves of ligand L^2	**Figure S18**
20. TG-DTG curves of $[CuL^1(NO_3)_2]_n$	**Figure S19**
21. TG-DTG curves of $[ZnL^1(NO_3)_2]_n$	**Figure S20**
22. Data extracted from TG-DTG experiments.	**Table S2**
23. Maldi-MS spectrum of bisazide 2.	**Figure S21**
24. Maldi-MS spectrum of L^1.	**Figure S22**
25. Maldi-MS spectrum of L^2.	**Figure S23**
26. Maldi-MS spectrum of $[CuL^1(NO_3)_2]_n$.	**Figure S24**
27. Maldi-MS spectrum of $[ZnL^1(NO_3)_2]_n$	**Figure S25**
28. XPS spectra of $[CuL^1(NO_3)_2]_n$, full scan, C1s, N1s, O1s and Cu2p (in this order).	**Figure S26**.
29. XPS spectra of $[ZnL^1(NO_3)_2]_n$, full scan, C1s, N1s, O1s and Zn2p (in this order).	**Figure S27**

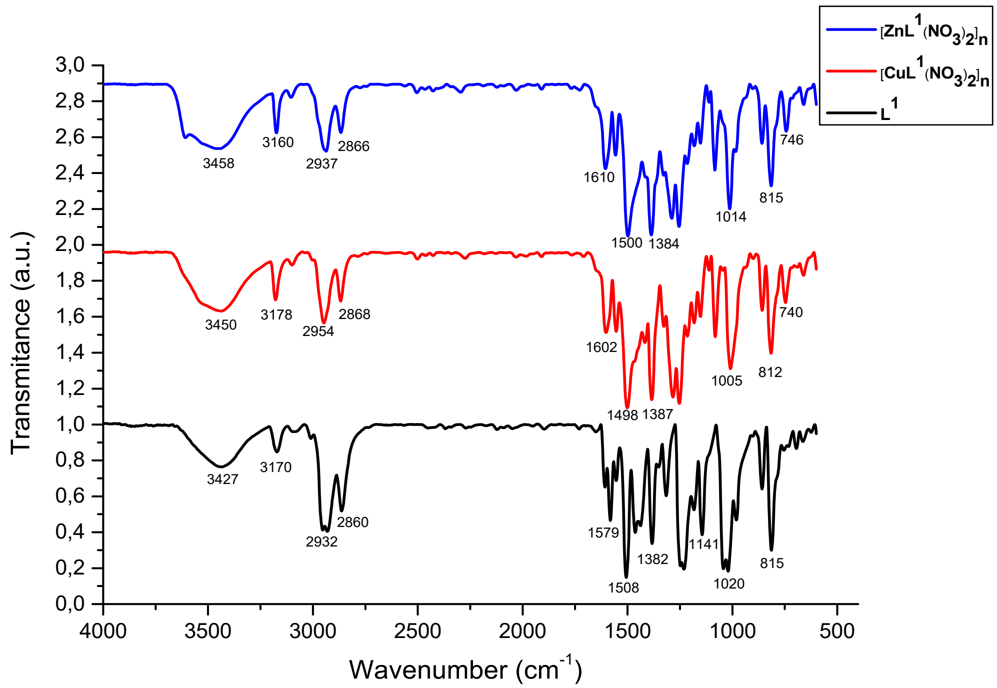

Figure S1. FT-IR spectra of ligand L¹, [CuL¹(NO₃)₂]ₙ and [ZnL¹(NO₃)₂]ₙ

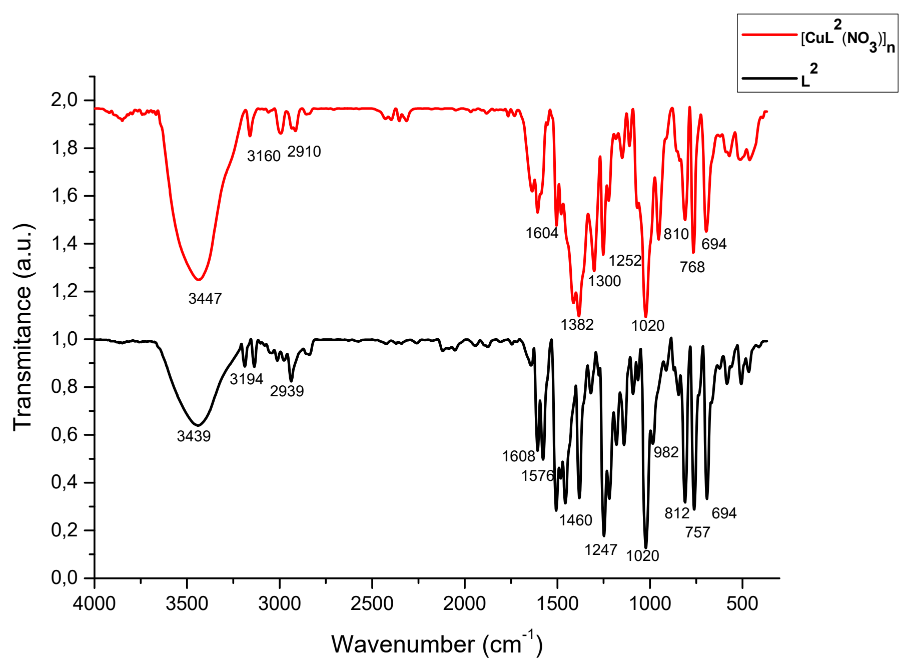

Figure S2. FT-IR spectra of ligand L^2 and $[CuL^2NO_3]_n$ complex.

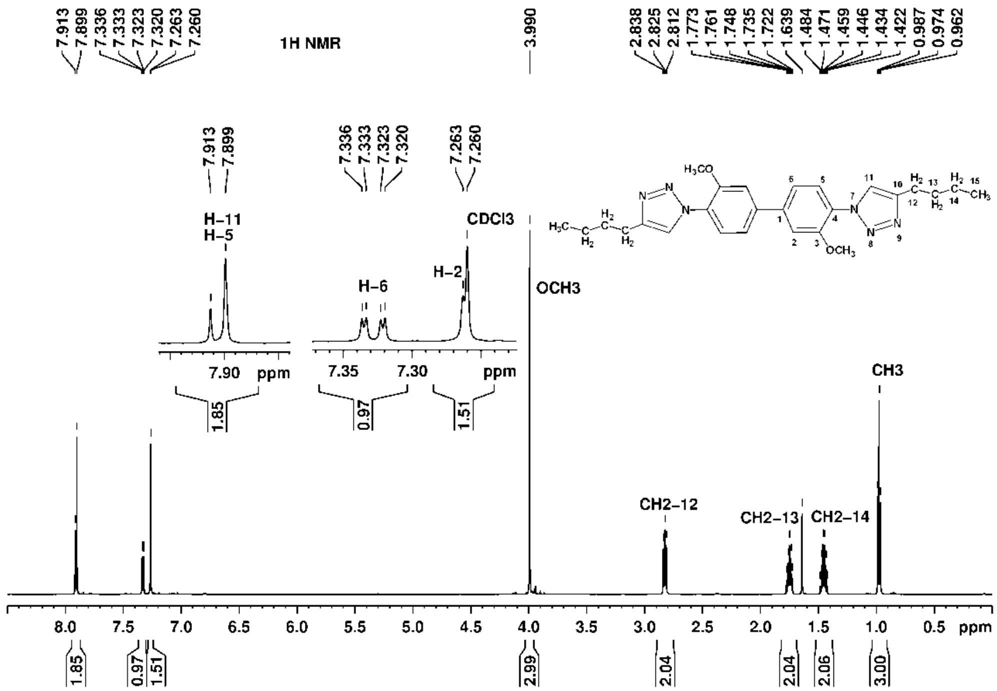

Figure S3. ^{1}H-NMR spectrum corresponding to compound L^1, recorded in $CDCl_3$, at 600.1 MHz. Signals assignments are annotated on the figure.

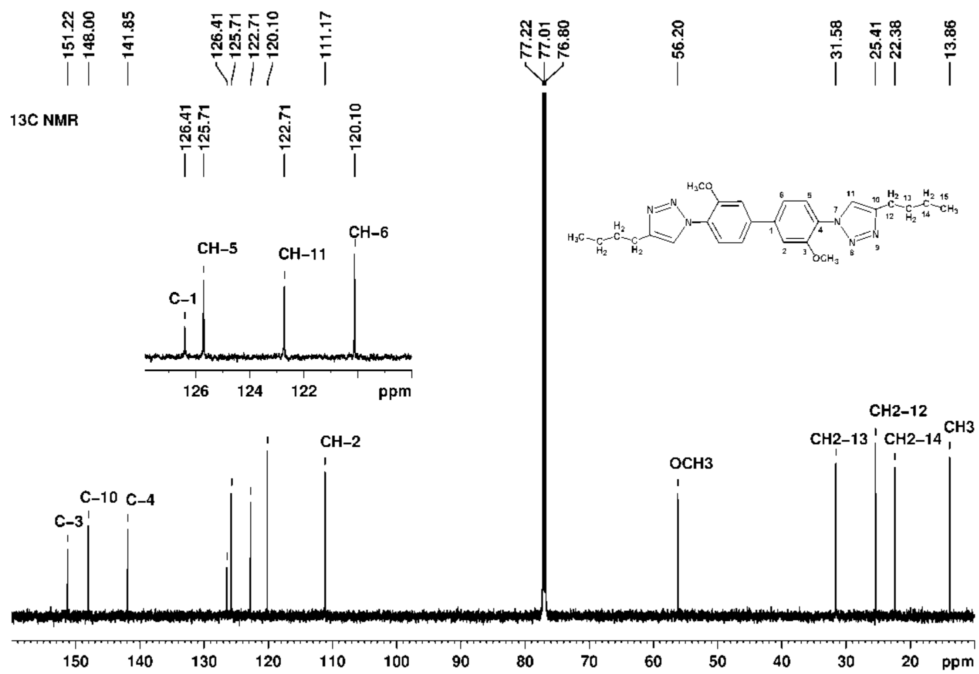

Figure S4. ^{13}C-NMR spectrum corresponding to compound L^1, recorded in $CDCl_3$, at 150.9 MHz. Signals assignments are annotated on the figure.

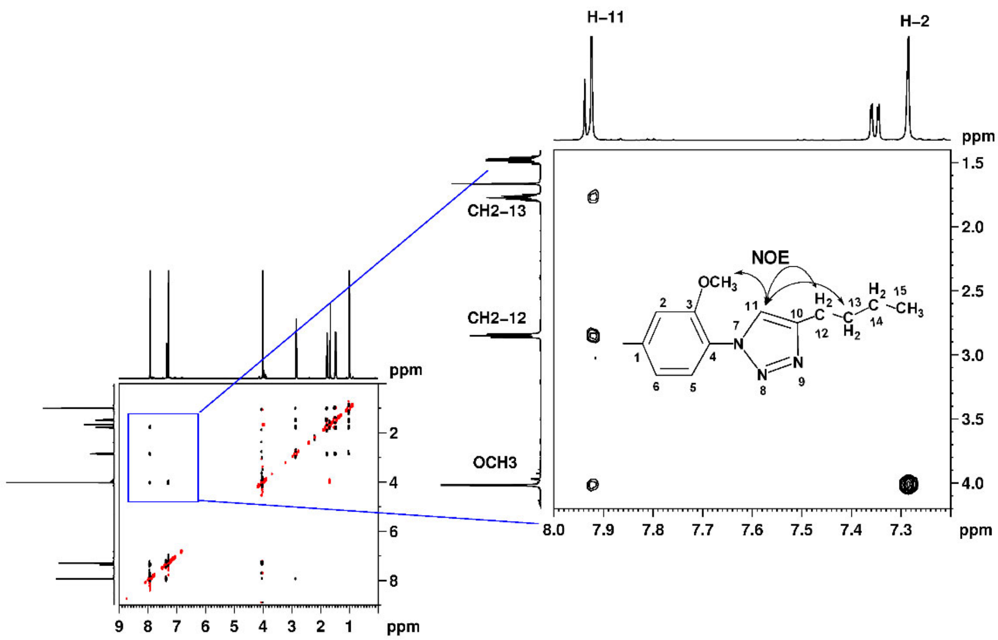

Figure S5. H,H-NOESY spectrum recorded for compound L[1], with the insert showing the NOE correlation signals between 1,2,3-triazole proton and methoxy and butyl protons.

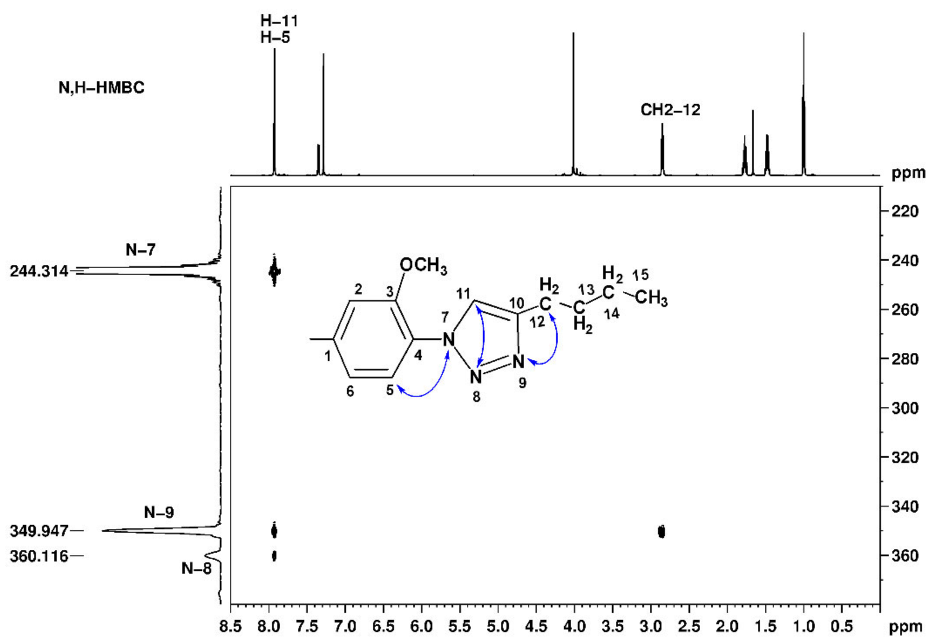

Figure S6. Detailed spectral region of ^{1}H,^{15}N-HMBC spectrum corresponding to compound L[1], showing the proton-nitrogen two and three bonds couplings used to determine the chemical shifts values for nitrogen atoms.

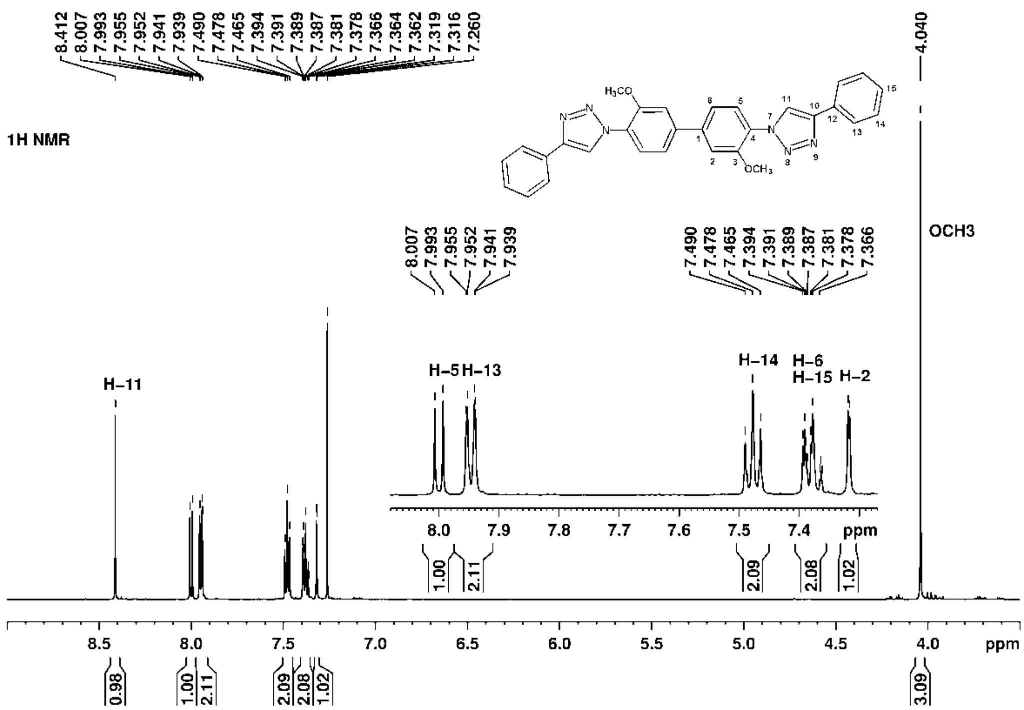

Figure S7. ^{1}H-NMR spectrum corresponding to compound L^2, recorded in $CDCl_3$, at 600.1 MHz. Signals assignments are annotated on the figure.

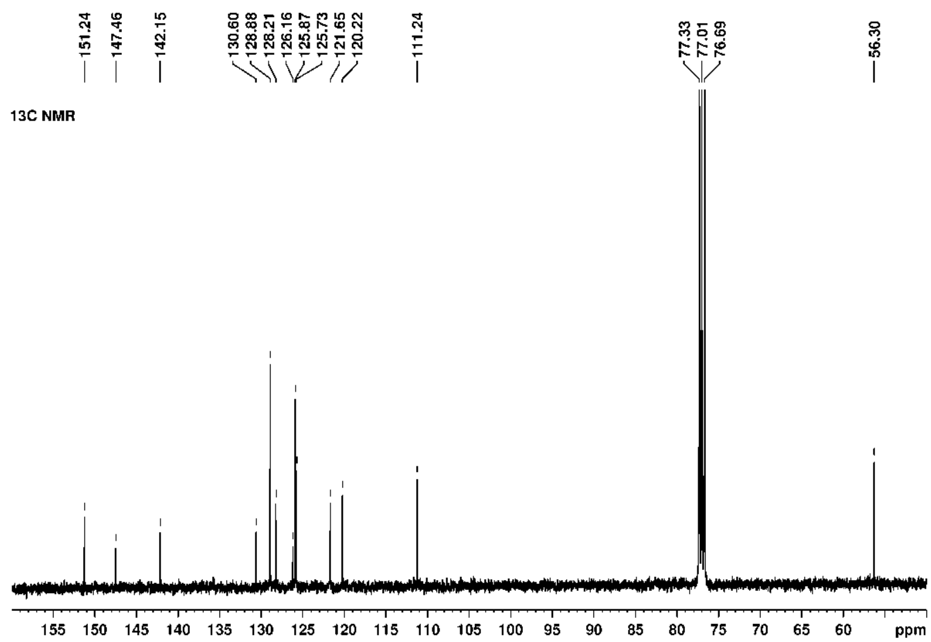

Figure S8. ^{13}C-NMR spectrum corresponding to compound L^2, recorded in $CDCl_3$, at 100.6 MHz.

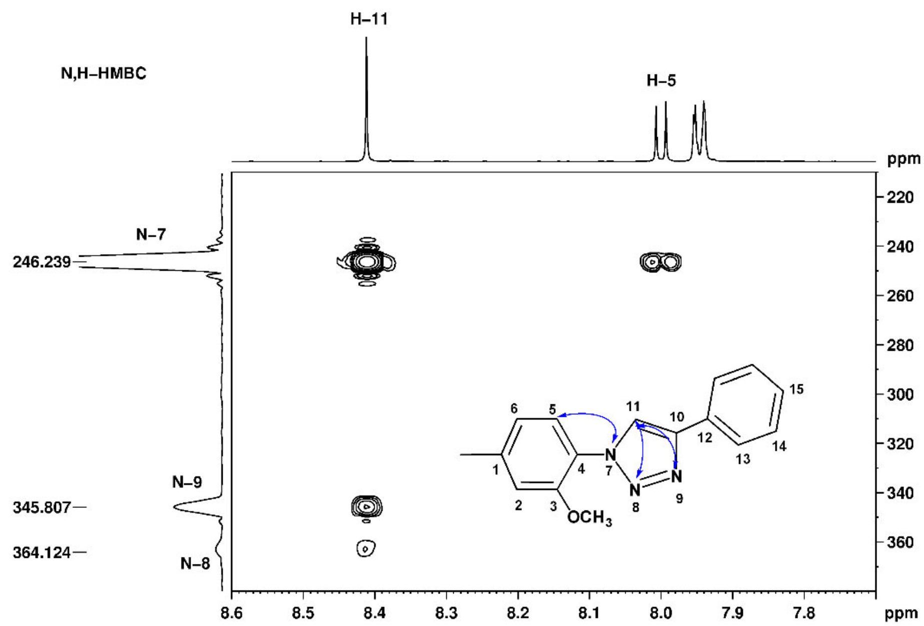

Figure S9. Detailed spectral region of $^{1}H,^{15}N$-HMBC spectrum corresponding to compound L^2, showing the proton-nitrogen two and three bounds couplings used to determine the chemical shifts values for nitrogen atoms.

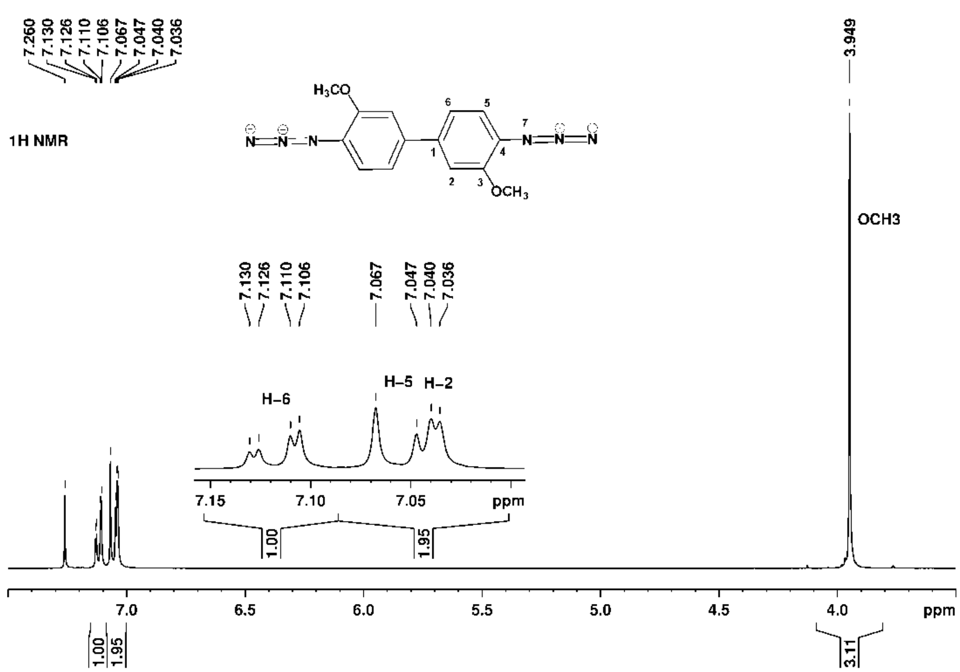

Figure S10. ^{1}H-NMR spectrum corresponding to bisazide **2**, recorded in $CDCl_3$, at 600.1 MHz. Signals assignments are annotated on the figure.

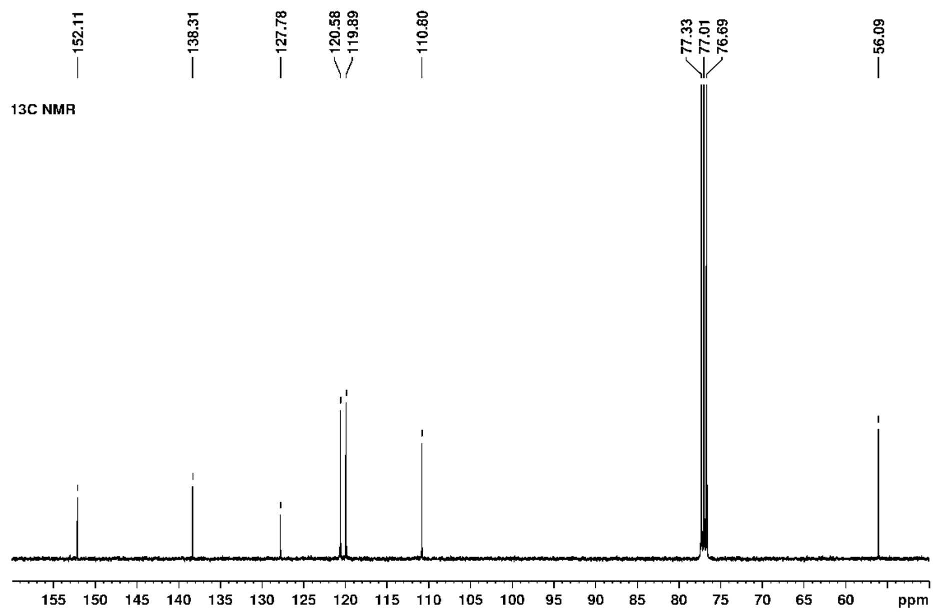

Figure S11. ^{13}C-NMR spectrum corresponding to bisazide **2**, recorded in $CDCl_3$, at 100.6 MHz.

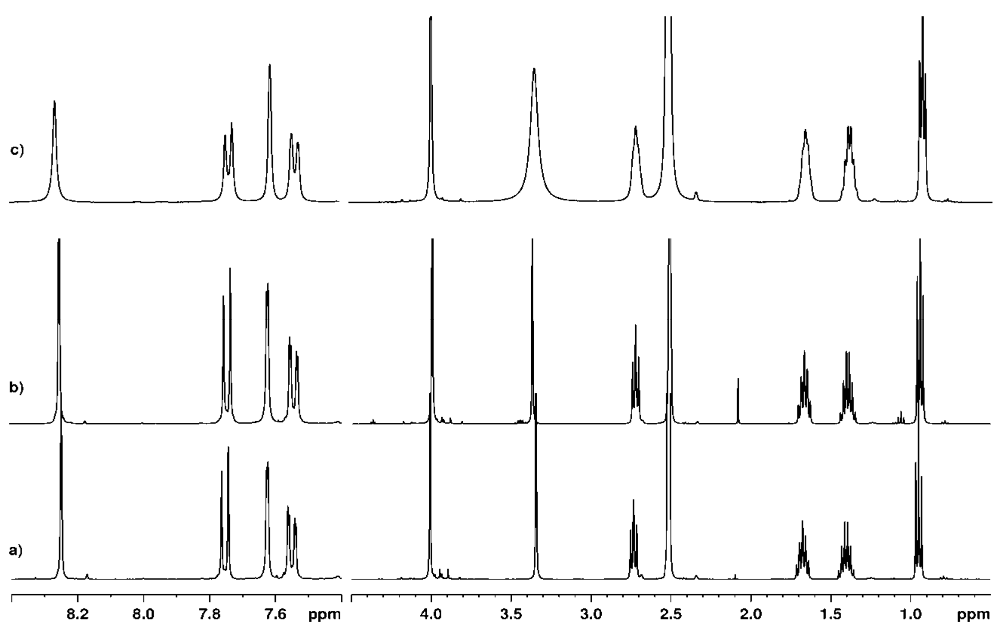

Figure S12. Overlapped ^{1}H-NMR spectra recorded at 400.1 MHz, in DMSO-d_6, for free L^1 (a), $[ZnL^1(NO_3)_2]_n$ complex (b) and $[CuL^1(NO_3)_2]_n$ complex (c). For copper complex, significant line broadening causing the modification of splitting patterns is observed for all the signals.

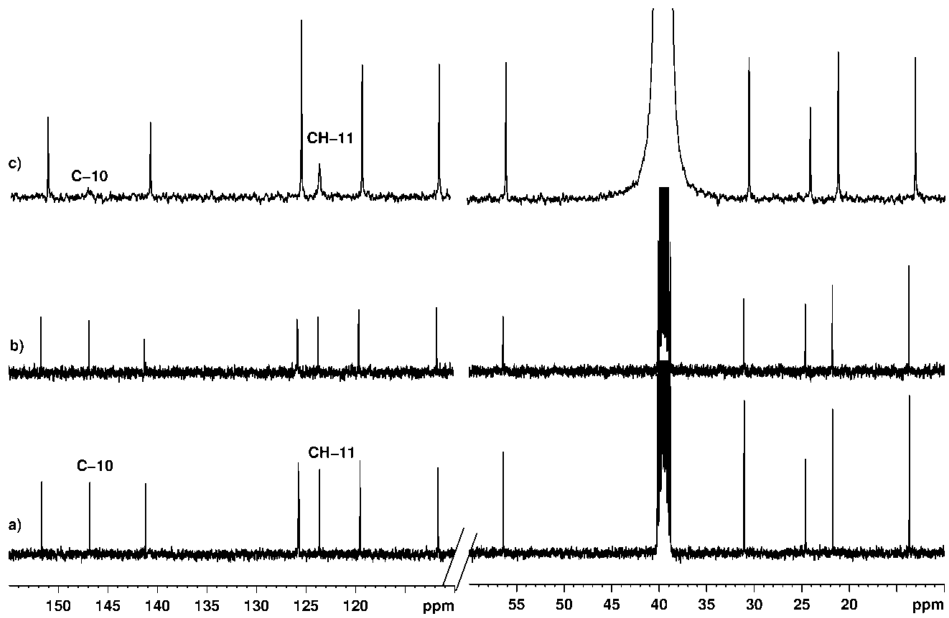

Figure S13. Overlapped ^{13}C-NMR spectra recorded at 100.6 MHz, in DMSO-d_6, for free L^1 (a), $[ZnL^1(NO_3)_2]_n$ complex (b) and $[CuL^1(NO_3)_2]_n$ complex (c). For copper complex, significant line broadening is observed for 1,2,3-triazole cycle carbons.

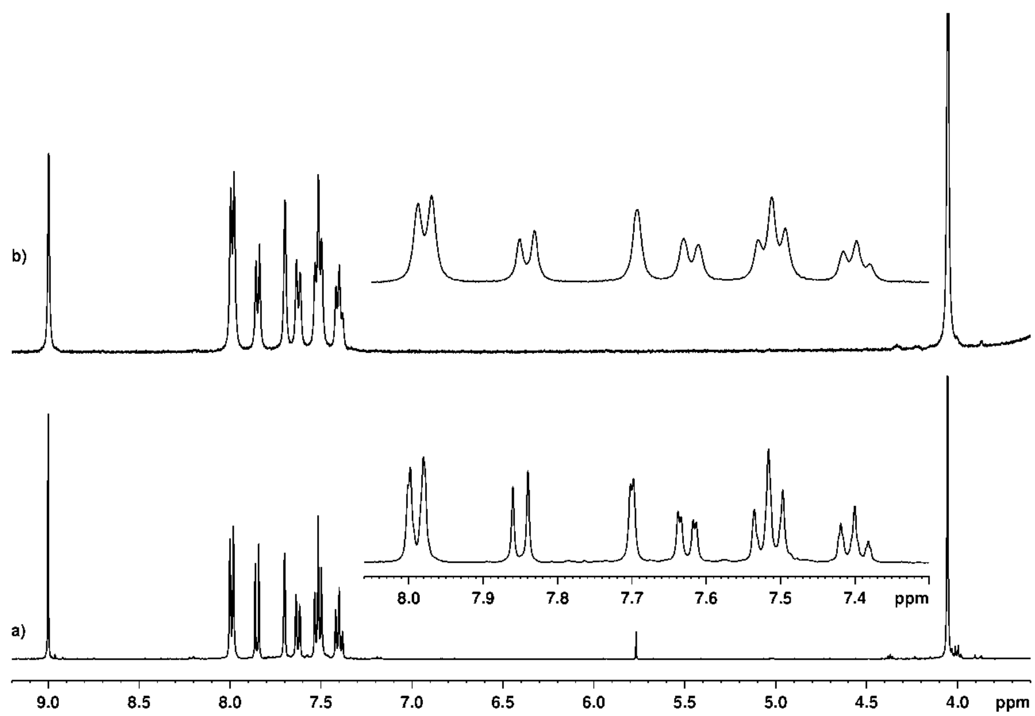

Figure S14. Overlapped ^{1}H-NMR spectra recorded at 400.1 MHz, in DMSO-d_6, for free L^2 (a) and $[CuL^2NO_3]$ complex (b). For copper complex, significant line broadening causing the modification of splitting patterns is observed for two signals.

Table S1. Bond distances (Å) and angles (°)

$[CuL^2NO_3]_n$ complex

C1-C2	1.378(6)	C19-C19[2]	1.492(8)
C1-C6	1.393(5)	C19-C20	1.395(6)
C1-N3	1.431(5)	C20-C21	1.372(6)
C2-C3	1.365(6)	C21-O2	1.368(5)
C3-C4	1.380(6)	C22-O2	1.407(5)
C4-C4[1]	1.478(8)	C23-C24	1.355(6)
C4-C5	1.398(5)	C23-N6	1.345(5)
C5-C6	1.381(6)	C24-C25	1.479(6)
C6-O1	1.349(5)	C24-N4	1.362(5)
C7-O1	1.443(5)	C25-C26	1.377(7)
C8-C9	1.361(6)	C25-C30	1.3916)
C8-N3	1.351(5)	C26-C27	1.380(7)
C9-C10	1.475(6)	C27-C28	1.381(8)
C9-N1	1.367(5)	C28-C29	1.370(8)
C10-C11	1.391(6)	C29-C30	1.374(7)
C10-C15	1.369(6)	Cu1-N1	1.908(4)
C11-C12	1.372(7)	Cu1-N4	1.933(3)
C12-C13	1.368(8)	Cu1-O3	2.140(5)
C13-C14	1.371(7)	N1-N2	1.316(5)
C14-C15	1.388(6)	N2-N3	1.340(5)
C16-C17	1.386(6)	N4-N5	1.313(5)
C16-C21	1.395(5)	N5-N6	1.329(5)
C16-N6	1.433(5)	N7-O3	1.193(6)
C17-C18	1.353(6)	N7-O4	1.238(6)
C18-C19	1.382(6)	N7-O5	1.213(6)

Symmetry codes: [1] $1-x, 2-y, -z$; [2] $1-x, 1-y, 3-z$

C2-C1-C6	119.4(4)	O2-C21-C16	115.6(4)
C2-C1-N3	117.7(4)	O2-C21-C20	125.9(4)
C6-C1-N3	123.0(4)	N6-C23-C24	105.7(4)
C3-C2-C1	121.1(4)	C23-C24-C25	130.2(4)
C2-C3-C4	121.6(4)	C23-C24-N4	106.9(4)
C3-C4-C4[1]	122.2(5)	N4-C24-C25	122.9(4)
C3-C4-C5	116.8(4)	C26-C25-C24	120.0(4)
C5-C4-C4[1]	121.0(5)	C26-C25-C30	119.4(4)
C6-C5-C4	122.6(4)	C30-C25-C24	120.6(5)

C5-C6-C1	118.5(4)	C27-C26-C25	120.7(5)
O1-C6-C1	116.6(4)	C26-C27-C28	119.6(6)
O1-C6-C5	124.9(4)	C29-C28-C27	119.7(5)
N3-C8-C9	106.3(4)	C28-C29-C30	121.0(5)
C8-C9-C10	130.8(4)	C29-C30-C25	119.5(5)
C8-C9-N1	106.6(4)	C9-N1-Cu1	136.9(3)
N1-C9-C10	122.5(4)	N2-N1-C9	110.0(3)
C11-C10-C9	118.9(4)	N2-N1-Cu1	113.1(3)
C15-C10-C9	122.8(4)	N1-N2-N3	106.8(3)
C15-C10-C11	118.3(4)	C8-N3-C1	132.4(3)
C12-C11-C10	120.1(5)	N2-N3-C1	117.3(3)
C13-C12-C11	121.5(5)	N2-N3-C8	110.2(4)
C12-C13-C14	118.9(5)	C24-N4-Cu1	132.0(3)
C13-C14-C15	120.1(6)	N5-N4-C24	109.9(3)
C10-C15-C14	121.2(5)	N5-N4-Cu1	118.0(3)
C17-C16-C21	119.4(4)	N4-N5-N6	106.4(3)
C17-C16-N6	118.5(4)	C23-N6-C16	130.3(4)
C21-C16-N6	122.0(4)	N5-N6-C16	118.6(3)
C18-C17-C16	120.7(4)	N5-N6-C23	111.0(4)
C17-C18-C19	121.7(4)	O3-N7-O4	120.1(6)
C18-C19-C19[2]	122.1(5)	O3-N7-O5	121.2(6)
C18-C19-C20	117.0(4)	O5-N7-O4	118.7(6)
C20-C19-C19[2]	120.9(5)	C6-O1-C7	118.6(4)
C21-C20-C19	122.6(4)	C21-O2-C22	118.2(4)
C20-C21-C16	118.5(4)	N7-O3-Cu1	125.7(4)

Symmetry codes: [1] $1-x, 2-y, -z$; [2] $1-x, 1-y, 3-z$

$[ZnL^1(NO_3)_2]_n$ **complex**

C1-C2	1.378(3)	C9-C10	1.495(3)
C1-C6	1.392(3)	C9-N1	1.355(2)
C1-N3	1.439(2)	C10-C11	1.514(3)
C2-C3	1.380(3)	C11-C12	1.516(3)
C3-C4	1.388(3)	C12-C13	1.516(3)
C4-C4[2]	1.495(4)	N1-N2	1.321(2)
C4-C5	1.389(3)	N1-Zn1	1.9985(17)
C5-C6	1.392(3)	N2-N3	1.340(2)
C6-O1	1.412(13)	N4-O2	1.287(3)
C7-O1	1.385(18)	N4-O3	1.214(3)
C8-C9	1.359(3)	N4-O4	1.236(3)

C8-N3	1.352(2)	O2-Zn1	1.996(3)

Symmetry codes: [1] $1-x, 2-y, 1-z$

C2-C1-C6	119.50(19)	C9-C10-C11	114.69(18)
C2-C1-N3	119.15(18)	C10-C11-C12	110.9(18)
C6-C1-N3	121.36(19)	C13-C12-C11	113.3 (2)
C1-C2-C3	120.8(2)	C9-N1-Zn1	127.32(14)
C2-C3-C4	120.9(2)	N2-N1-C9	110.82(17)
C3-C4-C4[2]	121.6(2)	N2-N1-Zn1	121.86(13)
C5-C4-C3	117.85(19)	N1-N2-N3	105.6(16)
C5-C4-C4[2]	120.5(2)	C8-N3-C1	131.64(17)
C4-C5-C6	121.78(19)	N2-N3-C1	117.37(17)
C5-C6-C1	119.1(2)	N2-N3-C8	110.99(17)
O1-C6-C1	116.7(10)	O3-N4-O2	121.9(3)
O1-C6-C5	123.0(11)	O3-N4-O4	125.1(3)
N3-C8-C9	105.8(18)	O4-N4-O2	112.9(3)
C8-C9-C10	131.83(19)	C6-O1-C7	122.0(2)
N1-C9-C8	106.80(18)	N4-O2-Zn1	109.4(2)
N1-C9-C10	121.37(18)		

Symmetry codes: [1] $1-x, 2-y, 1-z$

Compound L[1]

C1-C2	1.408(9)	C15-C16	1.371(7)
C2-C3	1.549(8)	C16-C17	1.383(7)
C3-C4	1.466(7)	C17-C18	1.388(7)
C4-C5	1.485(7)	C17-N3	1.422(6)
C5-C6	1.345(13)	C18-C19	1.383(7)
C5-N4	1.391(8)	C18-O1	1.365(6)
C6-N6	1.312(12)	C20-O1	1.421(6)
C7-C8	1.365(6)	C21-C22	1.343(8)
C7-C12	1.386(6)	C21-N3	1.331(6)
C7-N6	1.423(6)	C22-C23	1.504(8)
C8-C9	1.371(7)	C22-N1	1.355(7)
C9-C10	1.397(7)	C23-C24	1.492(10)
C10-C11	1.389(6)	C24-C25	1.539(10)
C10-C14	1.481(7)	C25-C26	1.529(10)
C11-C12	1.394(7)	N1-N2	1.309(6)
C12-O2	1.365(5)	N2-N3	1.344(6)

C13-O2	1.420(6)	N4-N5	1.289(13)
C14-C15	1.381(7)	N5-N6	1.387(8)
C14-C19	1.386(7)		

C1-C2-C3	114.2(7)	C16-C17-N3	119.4(5)
C4-C3-C2	112.0(6)	C18-C17-N3	122.3(5)
C3-C4-C5	116.1(6)	C19-C18-C17	120.1(5)
C6-C5-C4	133.6(7)	O1-C18-C17	116.5(5)
N4-C5-C4	120.8(7)	O1-C18-C19	123.4(5)
N6-C6-C5	108.7(13)	C18-C19-C14	121.7(5)
C8-C7-C12	119.0(5)	N3-C21-C22	105.7(5)
C8-C7-N6	119.5(5)	C21-C22-C23	130.0(6)
C12-C7-N6	121.5(5)	C21-C22-N1	108.3(6)
C7-C8-C9	122.0(5)	N1-C22-C23	121.7(6)
C8-C9-C10	120.3(5)	C24-C23-C22	112.6(14)
C9-C10-C14	121.3(5)	C23-C24-C25	108(2)
C11-C10-C9	117.8(5)	C26-C25-C24	110(3)
C11-C10-C14	120.9(5)	N2-N1-C22	108.7(5)
C10-C11-C12	121.2(5)	N1-N2-N3	106.8(5)
C7-C12-C11	119.7(5)	C21-N3-C17	130.3(5)
O2-C12-C7	117.9(5)	C21-N3-N2	110.4(5)
O2-C12-C11	122.5(5)	N2-N3-C17	119.2(5)
C15-C14-C10	121.2(5)	N5-N4-C5	110.4(9)
C15-C14-C19	117.3(5)	N4-N5-N6	106.2(8)
C19-C14-C10	121.5(5)	C6-N6-C7	134.4(7)
C16-C15-C14	121.7(5)	N5-N6-C7	115.5(6)
C15-C16-C17	120.8(5)	C18-O1-C20	118.4(5)
C16-C17-C18	118.3(5)	C12-O2-C13	119.7(4)

$[CuL^1(NO_3)_2]_n$ complex

C1-C2	1.378(5)	C9-C10	1.496(5)
C1-C6	1.399(5)	C9-N1	1.354(4)
C1-N3	1.440(4)	C10-C11	1.521(5)
C2-C3	1.383(5)	C11-C12	1.521(5)
C3-C4	1.388(5)	C12-C13	1.522(5)
$C4-C4^2$	1.494(7)	$Cu1-N1^1$	2.018(3)

C4-C5	1.392(5)	Cu1-N1	2.018(3)
C5-C6	1.389(5)	Cu1-O4	1.959(3)
C6-O1	1.360(5)	Cu1-O4[1]	1.959(3)
C7-O1	1.427(4)	N1-N2	1.315(4)
C8-C9	1.367(5)	N2-N3	1.340(4)
C8-N3	1.359(4)		

Symmetry codes: [1] 2 – *x*, 1 – *y*, – *z*; [2] 2 – *x*, + *y*, ½ – *z*

C2-C1-C6	119.3(3)	C9-C10-C11	114.6(3)
C2-C1-N3	118.7(3)	C10-C11-C12	111.1(3)
C6-C1-N3	121.9(3)	C13-C12-C11	112.8(3)
C3-C2-C1	120.7(3)	C9-N1-Cu1	133.2(2)
C4-C3-C2	121.4(3)	N2-N1-C9	111.0(3)
C3-C4-C4[2]	122.0(4)	N2-N1-Cu1	115.3(2)
C3-C4-C5	117.4(3)	N1-N2-N3	106.0(3)
C5-C4-C4[2]	120.6(4)	C8-N3-C1	131.6(3)
C6-C5-C4	122.0(3)	N2-N3-C1	117.7(3)
C5-C6-C1	119.1(3)	N2-N3-C8	110.7(3)
O1-C6-C1	116.7(3)	N3-C8-C9	105.5(3)
O1-C6-C5	124.1(3)	C8-C9-C10	130.6(3)
N1-C9-C10	122.6(3)	N1-C9-C8	106.7(3)

Symmetry codes: [1] 2 – *x*, 1 – *y*, – *z*

Compound L^2

C1-C2	1.370(3)	C17-C18	1.378(3)
C1-C6	1.371(3)	C18-C19	1.390(3)
C1-C7	1.464(3)	C18-O2	1.359(2)
C2-C3	1.376(3)	C19-C20	1.367(3)
C3-C4	1.354(3)	C19-N6	1.430(2)
C4-C5	1.358(3)	C20-C21	1.379(3)
C5-C6	1.381(3)	C22-O2	1.420(2)
C7-C8	1.357(3)	C23-C24	1.362(3)
C7-N1	1.350(3)	C23-N6	1.335(2)
C8-N3	1.339(2)	C24-C25	1.458(3)
C9-C10	1.371(3)	C24-N4	1.363(3)
C9-C14	1.390(3)	C25-C26	1.387(3)
C9-N3	1.426(2)	C25-C30	1.381(3)
C10-C11	1.372(3)	C26-C27	1.375(3)

C11-C12	1.385(3)	C27-C28	1.371(3)
C12-C13	1.385(3)	C28-C29	1.366(3)
C12-C16	1.481(3)	C29-C30	1.371(3)
C13-C14	1.386(3)	N1-N2	1.305(3)
C14-O1	1.358(2)	N2-N3	1.350(2)
C15-O1	1.419(3)	N4-N5	1.310(2)
C16-C17	1.388(3)	N5-N6	1.356(2)
C16-C21	1.384(3)		

C2-C1-C6	117.6(2)	O2-C18-C19	116.36(19)
C2-C1-C7	120.8(2)	C18-C19-N6	119.05(19)
C6-C1-C7	121.6(2)	C20-C19-C18	120.25(19)
C1-C2-C3	121.2(2)	C20-C19-N6	120.7(2)
C4-C3-C2	120.5(2)	C19-C20-C21	120.6(2)
C3-C4-C5	119.6(2)	C20-C21-C16	120.2(2)
C4-C5-C6	120.0(2)	N6-C23-C24	106.2(2)
C1-C6-C5	121.3(2)	C23-C24-C25	130.1(2)
C8-C7-C1	131.1(2)	N4-C24-C23	107.19(19)
N1-C7-C1	121.7(2)	N4-C24-C25	122.7(2)
N1-C7-C8	107.25(19)	C26-C25-C24	120.6(2)
N3-C8-C7	106.7(2)	C30-C25-C24	121.4(2)
C10-C9-C14	119.06(19)	C30-C25-C26	117.9(2)
C10-C9-N3	118.39(19)	C27-C26-C25	120.7(2)
C14-C9-N3	122.55(19)	C28-C27-C26	120.5(2)
C11-C10-C9	121.3(2)	C29-C28-C27	119.2(2)
C10-C11-C12	120.8(2)	C28-C29-C30	120.8(2)
C11-C12-C13	117.79(19)	C29-C30-C25	120.9(2)
C11-C12-C16	120.66(19)	N2-N1-C7	109.49(19)
C13-C12-C16	121.55(19)	N1-N2-N3	107.60(18)
C12-C13-C14	121.7(2)	C8-N3-C9	132.89(19)
C13-C14-C9	119.29(19)	C8-N3-N2	108.96(17)
O1-C14-C9	117.16(18)	N2-N3-C9	118.07(18)
O1-C14-C13	123.5(2)	N5-N4-C24	109.76(18)
C17-C16-C12	119.0(2)	N4-N5-N6	106.52(17)
C21-C16-C12	122.2(2)	C23-N6-C19	128.91(18)
C21-C16-C17	118.8(2)	C23-N6-N5	110.36(17)
C18-C17-C16	121.2(2)	N5-N6-C19	120.72(18)
C17-C18-C19	118.9(2)	C14-O1-C15	118.51(17)

O2-C18-C17	124.7(2)	C18-O2-C22	117.90(17)

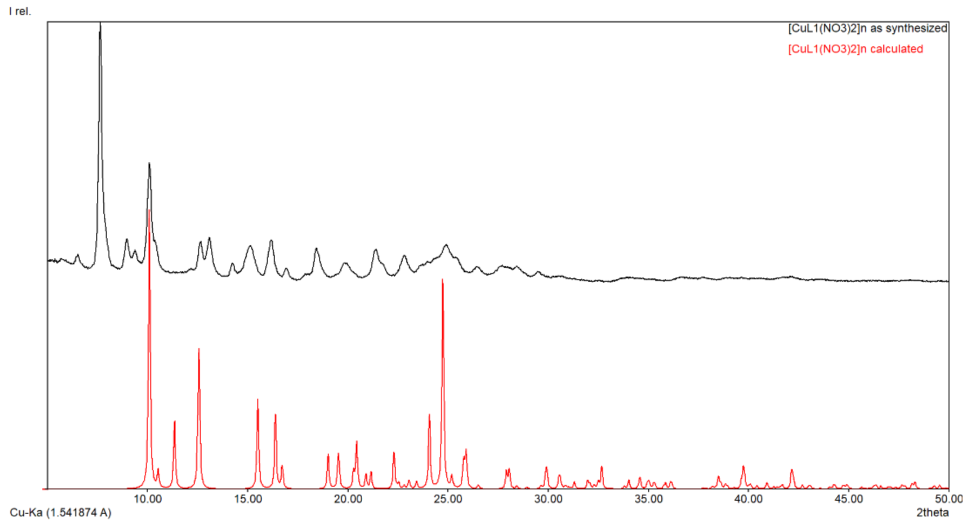

Figure S15. Powder XRD for $[CuL^1(NO_3)_2]_n$ complex. According to the EPR analysis, the large peak at approximatively 7.6 ° 2θ indicates the presence of binuclear complexes corresponding to dimers.

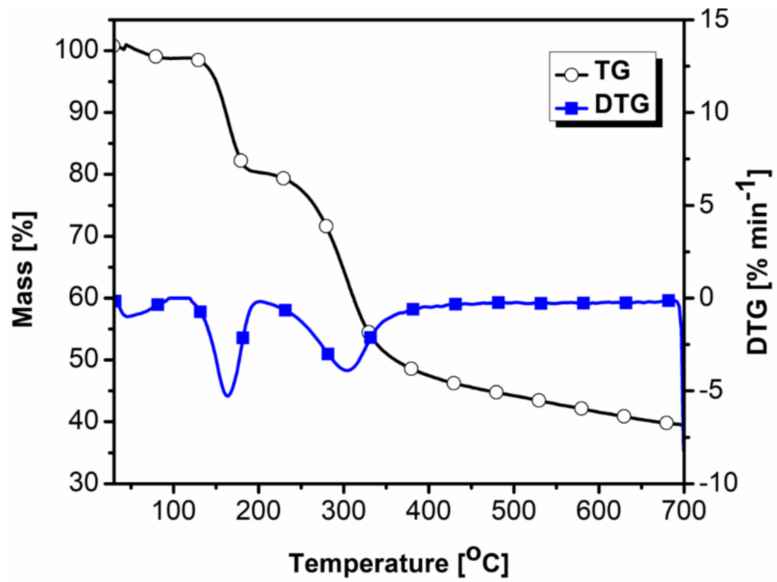

Figure S16. TG-DTG curves of bisazide 2.

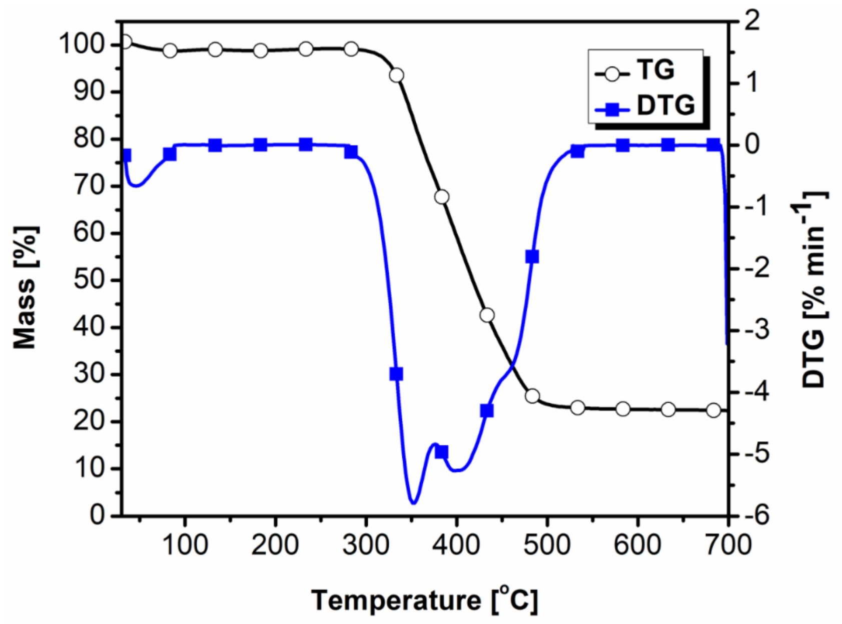

Figure S17. TG-DTG curves of ligand L[1].

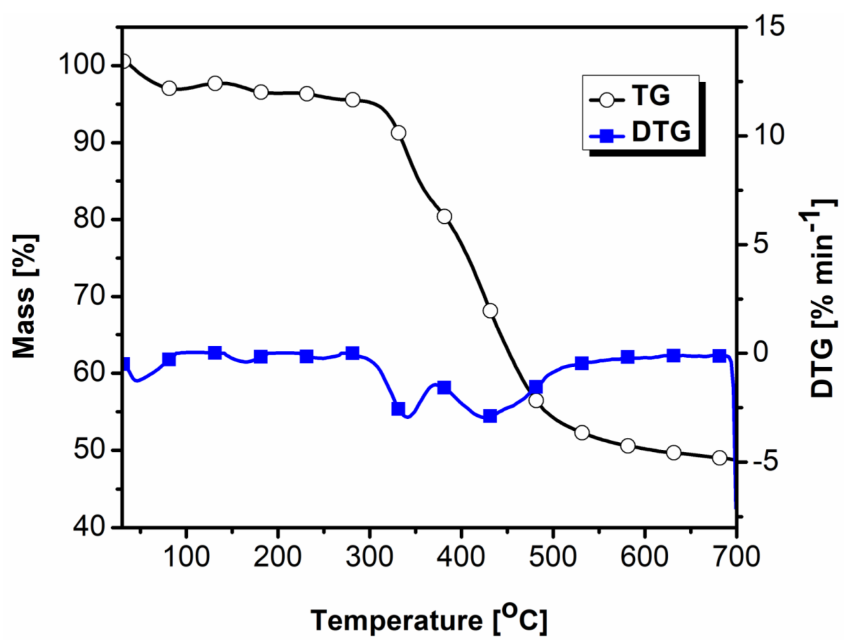

Figure S18. TG-DTG curves of ligand L[2].

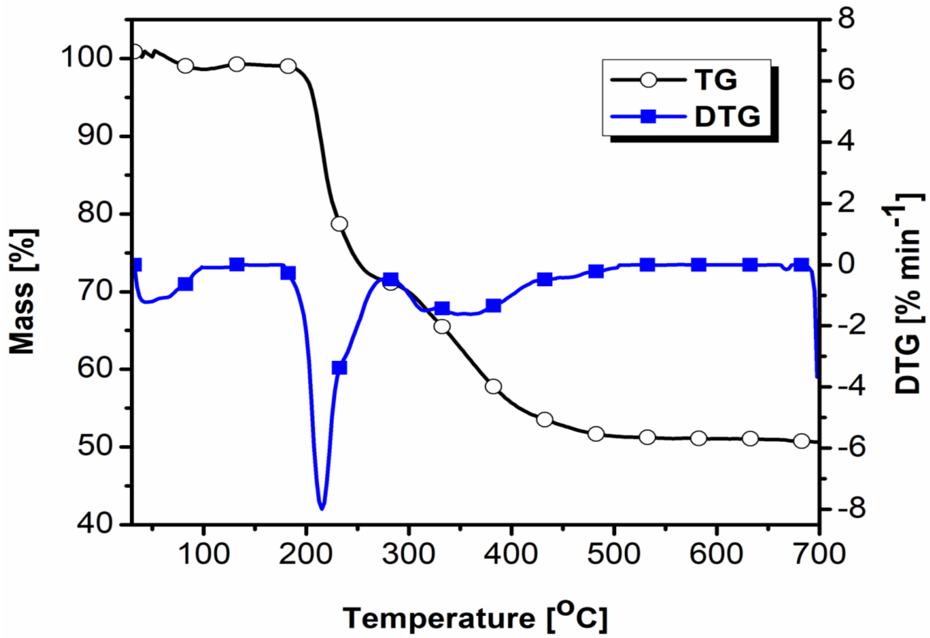

Figure S19. TG-DTG curves of $[CuL^1(NO_3)_2]_n$.

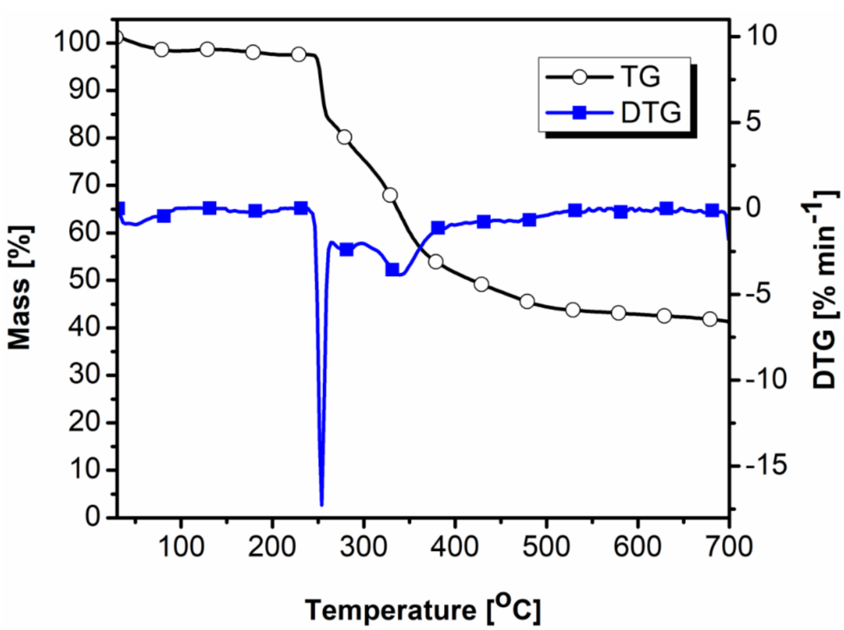

Figure S20. TG-DTG curves of $[ZnL^1(NO_3)_2]_n$.

Table S2. Data extracted from TG-DTG experiments.

Sample	Stage	T_{onset} (°C)	T_{max} (°C)	T_{endset} (°C)	W_m (%)	W_{rez} (%)
Bisazide 2	I	31	46	84	2.08	39.04
	II	133	164	183	18.93	
	III	246	304	339	39.36	
Ligand L^1	I	33	45	77	1.11	22
	II	318	352	366	25.44	
	III	366	400	424	27.85	
	IV	424	459	481	23.52	
Ligand L^2	I	29	46	83	2.97	48.28
	II	148	165	184	1.18	
	III	229	248	264	0.88	
	IV	307	341	354	12.96	
	V	377	425	491	32.89	
$[CuL^1(NO_3)_2]_n$	I	32	44	104	2.56	49.88
	II	201	215	224	18.01	
	III	224	239	258	8.10	
	IV	296	316	397	15.38	
	V	397	457	476	5.91	
$[ZnL^1(NO_3)_2]_n$	I	41	39	88	1.42	41.02
	II	150	190	209	1.01	
	III	248	254	257	14.65	
	IV	270	284	301	9.18	
	V	317	339	366	18.76	
	VI	366	470	500	13.89	

T_{onset} – onset thermal degradation temperature;
T_{max} – temperature that corresponds to the maximum rate of decomposition for each stage evaluated from the peaks of the DTG curves;
T_{endset} – endset thermal degradation temperature;
W_m – mass loss rate corresponding to each thermal degradation stage;
W_{rez} – percentage of residue remained at the end of the thermal degradation process (700°C).

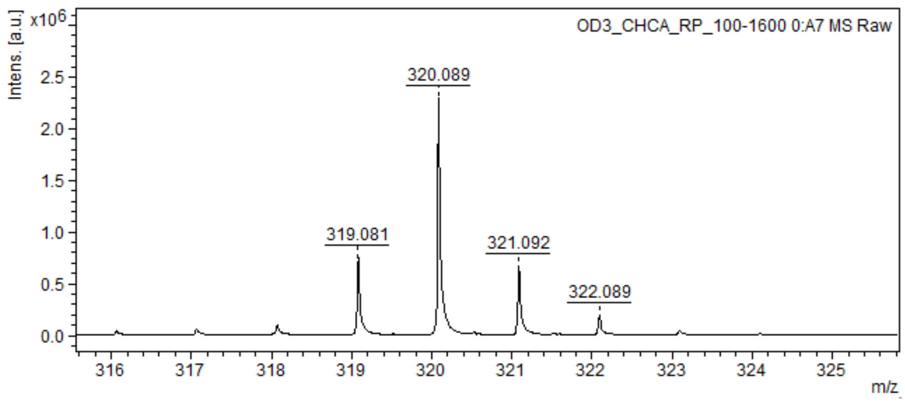

Figure S21. Maldi-MS spectrum of bisazide 2.

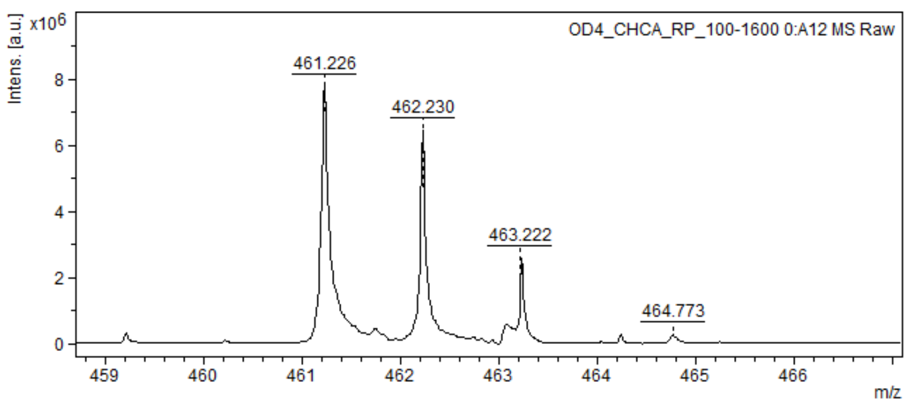

Figure S22. Maldi-MS spectrum of L^1.

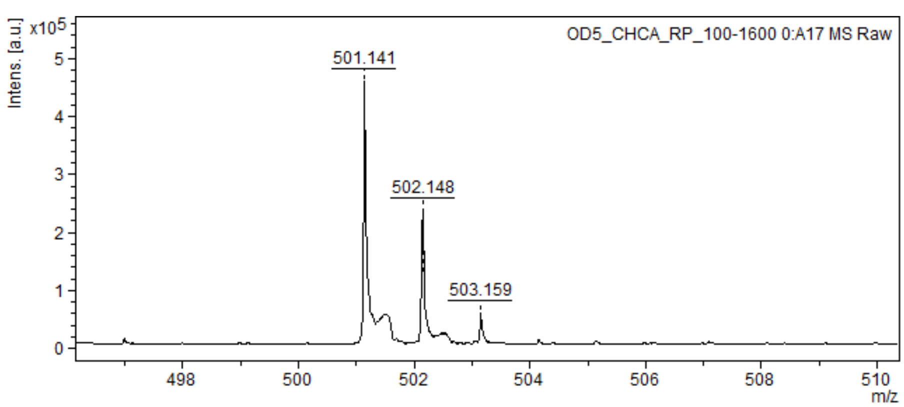

Figure S23. Maldi-MS spectrum of L^2.

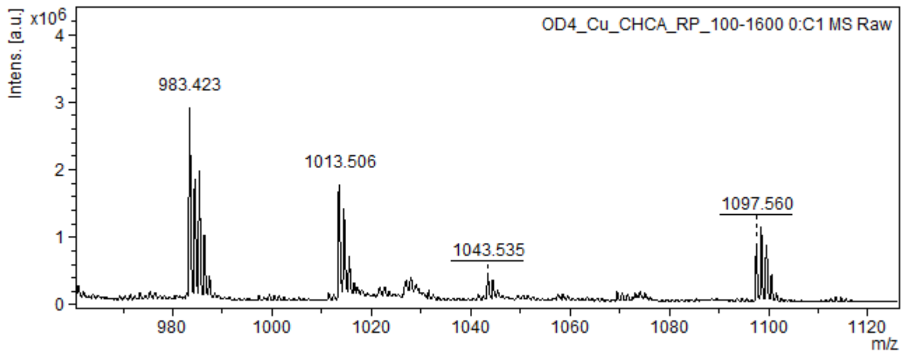

Figure S24. Maldi-MS spectrum of $[CuL^1(NO_3)_2]_n$.

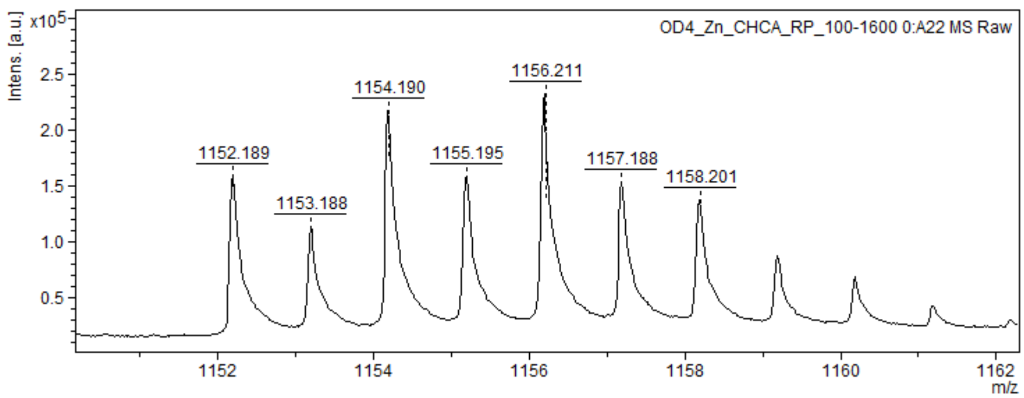

Figure S25. Maldi-MS spectrum of $[ZnL^1(NO_3)_2]_n$.

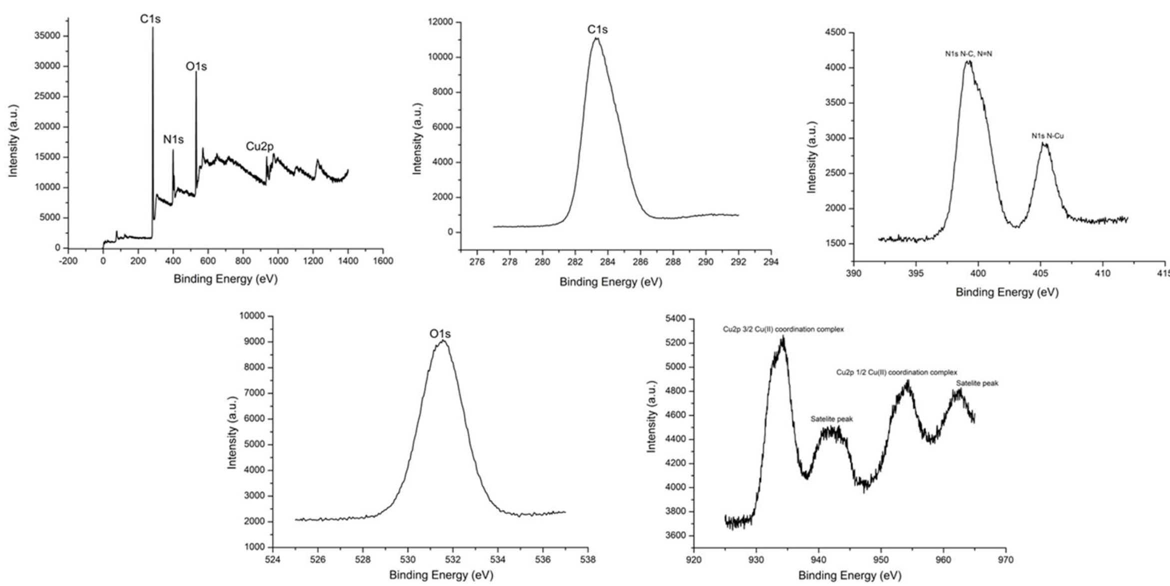

Figure S26. XPS spectra of $[CuL^1(NO_3)_2]_n$, full scan, C1s, N1s, O1s and Cu2p (in this order).

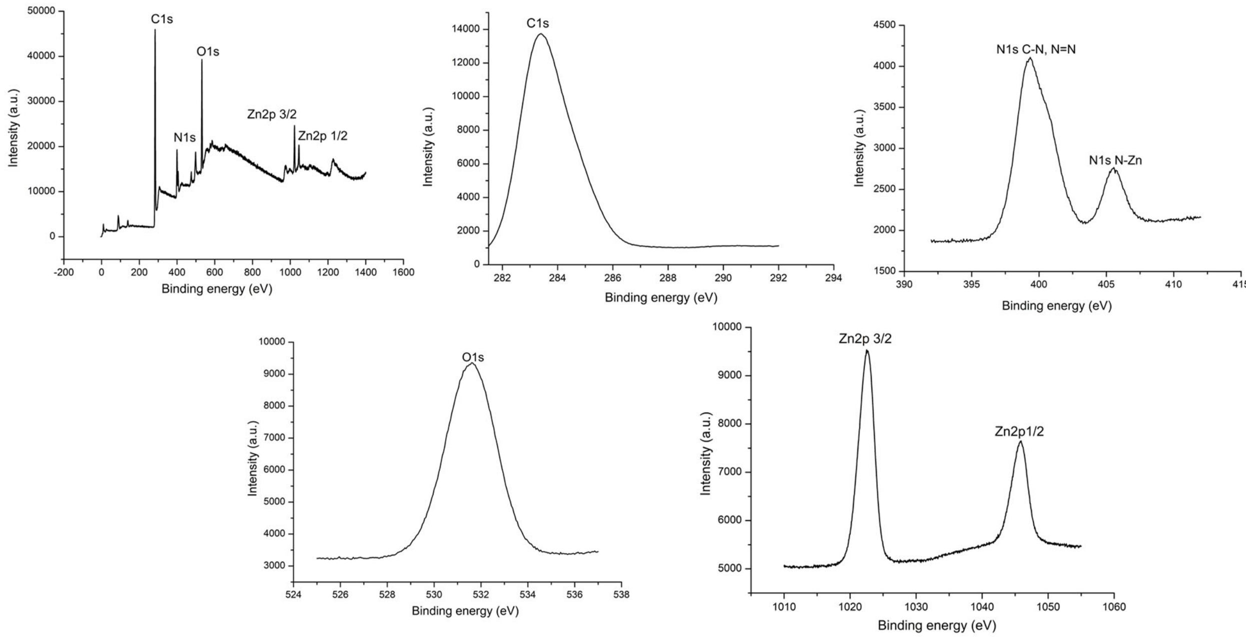

Figure S27. XPS spectra of $[ZnL^1(NO_3)_2]_n$, full scan, C1s, N1s, O1s and Zn2p (in this order).